

Local Stellar Kinematics from RAVE data - VII. Metallicity Gradients from Red Clump Stars

Ö. Önal Taş^{1*}, S. Bilir², G. M. Seabroke³, S. Karaali², S. Ak², T. Ak², and Z. F. Bostancı²

¹Istanbul University, Graduate School of Science and Engineering, Department of Astronomy and Space Sciences, 34116, Beyazıt, Istanbul, Turkey

²Istanbul University, Faculty of Science, Department of Astronomy and Space Sciences, 34119, Beyazıt, Istanbul, Turkey

³University College London, Mullard Space Science Laboratory, Holmbury St Mary, Dorking, RH5 6NT, United Kingdom

Abstract

We investigate the Milky Way Galaxy’s radial and vertical metallicity gradients using a sample of 47,406 red clump stars from the RAdial Velocity Experiment (RAVE) Data Release (DR) 4. This sample is more than twice the size of the largest sample in the literature investigating radial and vertical metallicity gradients. The absolute magnitude of Groenewegen (2008) is used to determine distances to our sample stars. The resulting distances agree with the RAVE DR4 distances (Binney et al., 2014) of the same stars. Our photometric method also provides distances to 6185 stars that are not assigned a distance in RAVE DR4. The metallicity gradients are calculated with their current orbital positions (R_{gc} and Z) and with their orbital properties (mean Galactocentric distance, R_m and z_{max}), as a function of the distance to the Galactic plane: $d[Fe/H]/dR_{gc} = -0.047 \pm 0.003$ dex kpc^{-1} for $0 \leq |Z| \leq 0.5$ kpc and $d[Fe/H]/dR_m = -0.025 \pm 0.002$ dex kpc^{-1} for $0 \leq z_{max} \leq 0.5$ kpc. This reaffirms the radial metallicity gradient in the thin disc but highlights that gradients are sensitive to the selection effects caused by the difference between R_{gc} and R_m . The radial gradient is flat in the distance interval 0.5-1 kpc from the plane and then becomes positive greater than 1 kpc from the plane. The radial metallicity gradients are also eccentricity dependent. We showed that $d[Fe/H]/dR_m = -0.089 \pm 0.010$, -0.073 ± 0.007 , -0.053 ± 0.004 and -0.044 ± 0.002 dex kpc^{-1} for $e_p \leq 0.05$, $e_p \leq 0.07$, $e_p \leq 0.10$ and $e_p \leq 0.20$ sub-samples, respectively, in the distance interval $0 \leq z_{max} \leq 0.5$ kpc. Similar trend is found for vertical metallicity gradients. Both the radial and vertical metallicity gradients are found to become shallower as the eccentricity of the sample increases. These findings can be used to constrain different formation scenarios of the thick and thin discs.

Keywords: The Galaxy: solar neighbourhood – disc – structure – stars: horizontal branch

1 Introduction

How galaxies formed in general and how our Galaxy formed specifically remain as unsolved problem in astrophysics. In order to understand the formation mechanisms and put constraints on simulations, Galactic archaeology relies on chemo-dynamical information of various tracer objects with different ages and chemical compositions with large baselines in the Galaxy. While overlapping properties make it difficult to disentangle the different components in the Galaxy, there are clear chemical and kinematical signatures in stars of the Solar neighborhood which change with increasing distances both in radial and vertical directions.

Sensitive metallicity gradients require tracer objects with well-measured distances and metallicities, which are obtained with either spectroscopic or photomet-

ric methods. Tracers include main-sequence stars, red clump (RC) stars, open or globular clusters, Cepheid variables, planetary nebulae, O-B type stars and HII regions. Various distance scales are used to determine radial and vertical metallicity gradients in the literature. In radial gradient calculations, if the tracer objects are distant, then the current distance from the Galactic centre is used (R_{gc}). If proper motions, radial velocities and distances of tracer objects are known, even though the objects are currently close to the Sun, then the mean Galactocentric distances of the tracer objects calculated from Galactic orbital parameters are used, under the assumption of that the metallicities are constant on the orbital integration timescale (R_m). Another distance scale presented to the literature is the guiding radius which is the distance of the tracer from the Galactic centre, if it is following its guiding centre, assumed to be a circular orbit (R_g). Also, current verti-

*ozgecan.onal@istanbul.edu.tr

cal distances and maximum vertical distances from the Galactic plane of the objects are generally considered in vertical metallicity gradient calculations.

Radial and vertical metallicity gradient studies that appeared in the literature almost in the last 15 years are listed in Tables 1 and 2, respectively. The organization of the metallicity gradient information is based on the distance indicators mentioned in the previous paragraph. According to Table 1, radial metallicity gradients tend to have steeper values near the Galactic plane and they flatten and even have positive values as the distance of the tracers from the Galactic plane increases. This behavior holds for different tracer objects, as well. Radial metallicity gradients of young objects show steeper values than the ones calculated from older objects. Similar results are also found in Table 1 for R_m . Vertical metallicity gradients are found to be steeper than their radial counterparts. And besides, absolute vertical metallicity gradients found for the Galactic disc ($z < 5$ kpc) give larger values than the ones found for the Galactic halo ($5 < z < 10$ kpc; see Table 2). This is also valid for objects with distances calculated from different methods.

The *Hipparcos* (ESA, 1997) era calculated accurate distance estimations for stars in the Solar neighborhood. High-resolution spectroscopic follow-up observations with ground-based telescopes allowed astronomers to determine more precise metallicity gradients for the small *Hipparcos* volume in the Solar neighborhood (i.e. Nordström et al., 2004). To increase this limited volume, astronomers initiated several photometric and spectroscopic sky surveys, such as the RAdial Velocity Experiment (RAVE; Steinmetz et al., 2006), the Sloan Extension for Galactic Understanding and Exploration (SEGUE; Yanny et al., 2009), the APO-Galactic Evolution Experiment (APOGEE; Majewski et al., 2010), the Large sky Area Multi Object fiber Spectroscopic Telescope (LAMOST; Zhao et al., 2012), the GALactic Archaeology with HERMES (GALAH; Zucker et al., 2012) and the Gaia-ESO Survey (GES; Gilmore et al., 2012). These surveys are designed to reveal the structure and test the formation mechanisms of the Milky Way's disc as well as to decode its evolution via metallicity, kinematics and dynamics of its stars.

According to stellar evolution models, a star within a mass range of 0.8 to 2.2 M_\odot could generate a helium (He) core mass of $\sim 0.45M_\odot$ after the hydrogen burning reactions ceased (Girardi, 1999). At this point, as stated by Carretta et al. (1999), when a star begins to evolve to the red giant phase, its surrounding envelope starts to interact with inner regions of the star, thus materials inside and in the outer surface of the star start mixing via convection processes. In a red giant, gravitational collapse of the star is supported via pressure of degenerate electrons, until the He core reaches 0.45 M_\odot . Then a series of He-flashes (Thomas, 1967) occurs

and breaks the degeneracy. Right after the removal of degeneracy, luminosity of the star suddenly drops and stable He burning reactions begin. Star's luminosity remains almost constant. At this stage, if a star is metal rich then it becomes an RC star, or if it is not metal rich then it becomes a member of the blue horizontal branch stars (Iben, 1991). Since the main-sequence mass of the RC stars are between 0.9 and 2.25 M_\odot according to theory (Eggleton, 1968), their main-sequence life times are between 13 to 1.3 Gyrs, respectively. Theory also predicts that the horizontal branch life times of stars is roughly 10% of the main-sequence life times. This is the reason why these stars form a clump structure in Hertzsprung-Russell diagrams. There has been much debate on the nature of the RC stars and their use as a standard candle since their discovery. Cannon (1970) suggested that RC stars could be used for distance determination as standard candles. There are several studies which show that the absolute magnitude of the RC stars in different parts of the electromagnetic spectrum is always the same (Paczynski & Stanek, 1998; Keenan & Barnbaum, 1999; Alves, 2000; Udalski, 2000; Groenewegen, 2008; Laney et al., 2012; Bilir et al., 2013a,b; Karaali et al., 2013; Yaz Gökçe et al., 2013): absolute magnitudes of the RC stars are in the near infrared K_s band, $M_{K_s} = -1.54 \pm 0.04$ mag (Groenewegen, 2008), and in I band $M_I = -0.23 \pm 0.03$ mag (Paczynski & Stanek, 1998). RC stars are common objects in the Solar neighborhood and their intrinsic brightness probes large distances, which enables us to investigate chemical gradients both in radial and vertical directions.

Rather than using spectroscopic parallaxes, we preferred photometric parallax method to calculate distances using the aforementioned well-known constant infrared absolute magnitude in the K_s band. Metallicity gradients are calculated for the current orbital positions of the stars as well as for their calculated complete orbit parameters. In metallicity gradient calculations we used the mean Galactocentric distance of stellar orbits (R_m) instead of guiding radius (R_g). One other aspect of the study is that the dynamical properties of each star are calculated with *galpy* library of Bovy (2015) using test particle integration for *MWPotential2014* potential.

In this paper, we present results on the metallicity gradients of the RC stars using data from RAVE DR4. In §2, we present the selection criteria of the RC stars and their distance, kinematic and dynamic calculations. In §3, we give the results on overall metallicity gradients obtained using various distance scales both in radial and vertical directions in the Galaxy. Also, a sub-sample separation with planar and vertical eccentricities are carried out and implications on radial migration of the RC stars are mentioned. We discussed the results on the RC stars in §4.

Table 1 Radial metallicity gradients appeared in the literature. Distances (R_{gc} , Z , R_m , z_{max} , R_g) in kpc, age (τ) in Gyr.

| Author | Tracer Object | $d[Fe/H]/dR_{gc}$ (dex kpc $^{-1}$) | Remark | $d[Fe/H]/dR_m$ (dex kpc $^{-1}$) | Remark | $d[Fe/H]/dR_g$ (dex kpc $^{-1}$) | Remark | Bibliographic Code |
|------------------------------|------------------|---|--------------------------------------|--------------------------------------|-----------------------------------|--------------------------------------|-----------------------------------|----------------------|
| Jacobson et al. (2016) | OC | -0.100 ± 0.020 | $6 < R_{gc} < 12$ | - | - | - | - | 2016A&A...591A...37J |
| Cunha et al. (2016) | OC/RG | -0.035 ± 0.007 | $6 < R_{gc} < 25$ | - | - | - | - | arXiv:1601.03099 |
| Netopil et al. (2016) | OC | -0.086 ± 0.009 | $5 < R_{gc} < 12$ | - | - | - | - | 2016A&A...585A.150N |
| Pievne et al. (2015) | FG MSs | -0.082 ± 0.013 | $1 < \tau < 2.5$ | - | - | - | - | 2016A&A...585A.150N |
| | | - | - | -0.083 ± 0.030 | $0 < z_{max} \leq 0.5$ ([Fe/H]) | -0.083 ± 0.030 | $0 < z_{max} \leq 0.5$ ([Fe/H]) | 2015PASA...32...43P |
| | | - | - | -0.048 ± 0.037 | $0.5 < z_{max} \leq 0.8$ ([Fe/H]) | -0.065 ± 0.039 | $0.5 < z_{max} \leq 0.8$ ([Fe/H]) | 2015PASA...32...43P |
| | | - | - | -0.063 ± 0.011 | $0 < z_{max} \leq 0.5$ ([M/H]) | -0.062 ± 0.018 | $0 < z_{max} \leq 0.5$ ([M/H]) | 2015PASA...32...43P |
| | | - | - | -0.028 ± 0.057 | $0.5 < z_{max} \leq 0.8$ ([M/H]) | -0.055 ± 0.045 | $0.5 < z_{max} \leq 0.8$ ([M/H]) | 2015PASA...32...43P |
| Huang et al. (2015) | RCs | -0.082 ± 0.003 | $ Z \leq 0.1$ | - | - | - | - | 2015RAA...15.1240H |
| | | -0.072 ± 0.004 | $0.1 < Z \leq 0.3$ | - | - | - | - | 2015RAA...15.1240H |
| | | -0.052 ± 0.005 | $0.3 < Z \leq 0.5$ | - | - | - | - | 2015RAA...15.1240H |
| | | -0.041 ± 0.005 | $0.5 < Z \leq 0.7$ | - | - | - | - | 2015RAA...15.1240H |
| | | -0.028 ± 0.005 | $0.7 < Z \leq 0.9$ | - | - | - | - | 2015RAA...15.1240H |
| | | -0.020 ± 0.007 | $0.9 < Z \leq 1.1$ | - | - | - | - | 2015RAA...15.1240H |
| Xiang et al. (2015) | Turnoff stars | -0.100 ± 0.003 | $ Z \leq 0.1; 2 < \tau < 16$ | - | - | - | - | 2015RAA...15.1209X |
| | | -0.050 ± 0.002 | $0.4 < Z \leq 0.6; 2 < \tau < 16$ | - | - | - | - | 2015RAA...15.1209X |
| | | -0.010 ± 0.002 | $0.9 < Z \leq 1.1; 2 < \tau < 16$ | - | - | - | - | 2015RAA...15.1209X |
| Recio-Blanco et al. (2014) | FGK MSs | -0.058 ± 0.008 | Thin disc ([M/H]) | - | - | - | - | 2014A&A...567A...5R |
| | | $+0.006 \pm 0.008$ | Thick disc ([M/H]) | - | - | - | - | 2014A&A...567A...5R |
| Mikolaitis et al. (2014) | FGK MSs | -0.044 ± 0.009 | Thin disc (main) | - | - | - | - | 2014A&A...572A..33M |
| | | -0.028 ± 0.018 | Thin disc (clean) | - | - | - | - | 2014A&A...572A..33M |
| | | $+0.008 \pm 0.007$ | Thick disc (main) | - | - | - | - | 2014A&A...572A..33M |
| | | $+0.008 \pm 0.007$ | Thick disc (clean) | - | - | - | - | 2014A&A...572A..33M |
| Genovali et al. (2014) | Cepheids | -0.021 ± 0.029 | $5 < R_{gc} < 19$ | - | - | - | - | 2014A&A...566A..37G |
| Andreuzzi et al. (2014) | OC | -0.04 | $6 < R_{gc} < 22$ | - | - | - | - | 2011MNRAS.412.1265A |
| Boeche et al. (2014) | RCs | - | - | - | - | -0.054 ± 0.004 | $0 < Z \leq 0.4$ | 2014A&A...568A..71B |
| | | - | - | - | - | -0.039 ± 0.004 | $0.4 < Z \leq 0.8$ | 2014A&A...568A..71B |
| | | - | - | - | - | -0.011 ± 0.008 | $0.8 < Z \leq 1.2$ | 2014A&A...568A..71B |
| | | - | - | - | - | $+0.047 \pm 0.018$ | $1.2 < Z \leq 2.0$ | 2014A&A...568A..71B |
| Hayden et al. (2014) | RG | -0.090 ± 0.002 | $0.00 < Z < 0.25; 0 < R_{gc} < 15$ | - | - | - | - | 2014AJ...147..116H |
| | | -0.076 ± 0.003 | $0.25 < Z < 0.50; 0 < R_{gc} < 15$ | - | - | - | - | 2014AJ...147..116H |
| | | -0.057 ± 0.003 | $0.50 < Z < 1.00; 0 < R_{gc} < 15$ | - | - | - | - | 2014AJ...147..116H |
| | | -0.030 ± 0.006 | $1.00 < Z < 2.00; 0 < R_{gc} < 15$ | - | - | - | - | 2014AJ...147..116H |
| Frinchaboy et al. (2013) | OC | -0.090 ± 0.030 | $7.9 < R_{gc} \leq 14.5$ | - | - | - | - | 2013ApJ...777L...1F |
| | | -0.200 ± 0.080 | $7.9 < R_{gc} \leq 10.0$ | - | - | - | - | 2013ApJ...777L...1F |
| | | -0.020 ± 0.090 | $10 < R_{gc} \leq 14.5$ | - | - | - | - | 2013ApJ...777L...1F |
| Boeche et al. (2013) | FG MSs | -0.059 ± 0.002 | $4.5 < R_{gc} < 9.5$ | - | - | -0.065 ± 0.003 | $0 < z_{max} \leq 0.4$ | 2013A&A...559A..59B |
| | | - | - | - | - | -0.059 ± 0.006 | $0.4 < z_{max} \leq 0.8$ | 2013A&A...559A..59B |
| | | - | - | - | - | $+0.006 \pm 0.015$ | $z_{max} > 0.8$ | 2013A&A...559A..59B |
| Carrell et al. (2012) | FGK MSs | $+0.015 \pm 0.005$ | $0.5 < Z < 1.0$, Isoc. method | - | - | - | - | 2012AJ...144..185C |
| | | $+0.017 \pm 0.005$ | $0.5 < Z < 1.0$, Photo. method | - | - | - | - | 2012AJ...144..185C |
| Bilir et al. (2012) | RCs | - | - | -0.041 ± 0.003 | $TD/D \leq 0.1$ | - | - | 2012MNRAS.421.3362B |
| | | - | - | -0.041 ± 0.007 | $e_v \leq 0.07$ | - | - | 2012MNRAS.421.3362B |
| | | - | - | -0.025 ± 0.040 | $e_v \leq 0.12$ | - | - | 2012MNRAS.421.3362B |
| | | - | - | $+0.022 \pm 0.006$ | $e_v \geq 0.25$ | - | - | 2012MNRAS.421.3362B |
| Coşkunoglu et al. (2012) | FG MSs | - | - | -0.043 ± 0.005 | F stars, $TD/D \leq 0.1$ | - | - | 2012MNRAS.419.2844C |
| | | - | - | -0.033 ± 0.007 | G stars, $TD/D \leq 0.1$ | - | - | 2012MNRAS.419.2844C |
| | | - | - | -0.051 ± 0.005 | F stars, $e_v \leq 0.04$ | - | - | 2012MNRAS.419.2844C |
| | | - | - | -0.020 ± 0.006 | G stars, $e_v \leq 0.04$ | - | - | 2012MNRAS.419.2844C |
| Cheng et al. (2012) | Turnoff stars | $-0.066^{+0.030}_{-0.044}$ | $0.15 < Z < 0.25$ | - | - | - | - | 2012ApJ...746..149C |
| | | $-0.064^{+0.015}_{-0.004}$ | $0.25 < Z < 0.50$ | - | - | - | - | 2012ApJ...746..149C |
| | | $-0.013^{+0.009}_{-0.002}$ | $0.50 < Z < 1.00$ | - | - | - | - | 2012ApJ...746..149C |
| | | $+0.028^{+0.007}_{-0.005}$ | $1.00 < Z < 1.50$ | - | - | - | - | 2012ApJ...746..149C |
| Yong et al. (2012) | OC | $-0.120^{+0.010}_{-0.140}$ | $\tau \geq 2.5; R_{gc} < 13$ | - | - | - | - | 2012AJ...144...95Y |
| Karataş & Klement (2012) | MSs | - | - | -0.070 ± 0.010 | $0 < z_{max} < 5$ | - | - | 2012NewA...17...22K |
| Luck & Lambert (2011) | Cepheids | -0.062 ± 0.002 | $4 < R_{gc} < 17$ | - | - | - | - | 2011AJ...142..136L |
| Ruchti et al. (2011) | RGB,RCs,HB,MS,SG | $+0.010 \pm 0.040$ | $5 < R_{gc} < 10, Z < 3$ | - | - | - | - | 2011ApJ...737...9R |
| Luck et al. (2011) | Cepheids | -0.055 ± 0.003 | $4 < R_{gc} < 16$ | - | - | - | - | 2011AJ...142...51L |
| Friel et al. (2010) | OC | -0.076 ± 0.018 | all sample | - | - | - | - | 2010AJ...139.1942F |
| Wu et al. (2009) | OC | -0.070 ± 0.011 | $6 \leq R_{gc} \leq 13.5$ | -0.082 ± 0.014 | $6 \leq R_m \leq 20$ | - | - | 2009MNRAS.399.2146W |
| Pedicelli et al. (2009) | Cepheids | -0.051 ± 0.004 | all sample | - | - | - | - | 2009A&A...504...81P |
| Magrini et al. (2009) | OC | -0.053 ± 0.029 | $7 < R_{gc} < 12, \tau \leq 0.8$ Gyr | - | - | - | - | 2009A&A...494...95M |
| Lemasle et al. (2008) | Cepheids | -0.052 ± 0.003 | $5 < R_{gc} < 17$ | - | - | - | - | 2008A&A...490..613L |
| Lemasle et al. (2007) | Cepheids | -0.061 ± 0.019 | $8 < R_{gc} < 12$ | - | - | - | - | 2007A&A...467..283L |
| Allende Prieto et al. (2006) | FG MSs | 0 | $1 < Z \leq 3$ | - | - | - | - | 2006ApJ...636..804A |
| Nordström et al. (2004) | FG MSs | - | - | -0.076 ± 0.014 | $\tau \leq 1.5$ | - | - | 2004A&A...418..989N |
| | | - | - | -0.099 ± 0.011 | $4 < \tau \leq 6$ | - | - | 2004A&A...418..989N |
| | | - | - | $+0.028 \pm 0.036$ | $\tau > 10$ | - | - | 2004A&A...418..989N |
| Chen et al. (2003) | OC | -0.063 ± 0.008 | $6 < R_{gc} < 15$ | - | - | - | - | 2003AJ...125.1397C |
| Hou (2002) | OC | -0.099 ± 0.008 | $6.5 < R_{gc} < 16$ | - | - | - | - | 2002ChJAA...2...17H |
| Friel et al. (2002) | OC | -0.060 ± 0.010 | $7 < R_{gc} < 16$ | - | - | - | - | 2002AJ...124.2693F |
| | | -0.023 ± 0.019 | $\tau < 2$ | - | - | - | - | 2002AJ...124.2693F |
| | | -0.053 ± 0.018 | $2 \leq \tau \leq 4$ | - | - | - | - | 2002AJ...124.2693F |
| | | -0.075 ± 0.019 | $\tau > 4$ | - | - | - | - | 2002AJ...124.2693F |
| Andrievsky et al. (2002) | Cepheids | -0.130 ± 0.030 | inner disc | - | - | - | - | 2002A&A...392..491A |

Abbreviations: Main Sequence Stars: MSs; Red Clump Stars: RCs; Red Giants: RG; Open Cluster: OC; Red Giant Branch: RGB; Horizontal Branch: HB; Sub-giant: SG

Table 2 Vertical metallicity gradients appeared in the literature. Distances (d , R_{gc} , Z , z_{max}) in kpc, age (τ) in Gyr.

| Author | Tracer Object | $d[Fe/H]/d Z $ (dex kpc $^{-1}$) | Remark | $d[Fe/H]/dz_{max}$ (dex kpc $^{-1}$) | Remark | Bibliographic Code |
|------------------------------|------------------|--------------------------------------|-------------------------------------|--|--------------------------|----------------------|
| Plevne et al. (2015) | F-G MSs | — | — | -0.176 ± 0.039 | $0 < z_{max} \leq 0.825$ | 2015PASA...32...43P |
| | | — | — | -0.119 ± 0.036 | $0 < z_{max} \leq 1.5$ | 2015PASA...32...43P |
| Xiang et al. (2015) | Turnoff stars | -0.110 ± 0.020 | $\tau > 11$ | — | — | 2015RAA...15.1209X |
| Huang et al. (2015) | RC | -0.206 ± 0.006 | $ Z \leq 1, 7 < R_{gc} \leq 8$ | — | — | 2015RAA...15.1240H |
| | | -0.116 ± 0.008 | $ Z \leq 1, 8 < R_{gc} \leq 9$ | — | — | 2015RAA...15.1240H |
| | | -0.052 ± 0.010 | $ Z \leq 1, 9 < R_{gc} \leq 10$ | — | — | 2015RAA...15.1240H |
| | | 0.000 ± 0.012 | $ Z \leq 1, 10 < R_{gc} \leq 11$ | — | — | 2015RAA...15.1240H |
| | | $+0.008 \pm 0.008$ | $ Z \leq 1, 11 < R_{gc} \leq 12$ | — | — | 2015RAA...15.1240H |
| | | $+0.057 \pm 0.012$ | $ Z \leq 1, 12 < R_{gc} \leq 13$ | — | — | 2015RAA...15.1240H |
| | | $+0.047 \pm 0.012$ | $ Z \leq 1, 13 < R_{gc} \leq 14$ | — | — | 2015RAA...15.1240H |
| Mikolaitis et al. (2014) | FGK MSs | -0.107 ± 0.009 | Thin disc (main) | — | — | 2014A&A...572A..33M |
| | | -0.057 ± 0.016 | Thin disc (clean) | — | — | 2014A&A...572A..33M |
| | | -0.072 ± 0.006 | Thick disc (main) | — | — | 2014A&A...572A..33M |
| | | -0.037 ± 0.016 | Thick disc (clean) | — | — | 2014A&A...572A..33M |
| Schlesinger et al. (2014) | G MSs | $-0.243^{+0.039}_{-0.053}$ | all sample | — | — | 2014ApJ...791..112S |
| Boeche et al. (2014) | RCs | -0.112 ± 0.007 | $0 < Z \leq 2$ | — | — | 2014A&A...568A..71B |
| Hayden et al. (2014) | RG | -0.305 ± 0.011 | $0 < Z \leq 2$ | — | — | 2014AJ...147..116H |
| Bergemann et al. (2014) | FGK MSs | -0.068 ± 0.014 | $ Z \leq 0.3$ | — | — | 2014A&A...565A..89B |
| | | -0.114 ± 0.009 | $0.3 < Z \leq 0.8$ | — | — | 2014A&A...565A..89B |
| Carrell et al. (2012) | FGK MSs | -0.113 ± 0.010 | $7 < R_{gc} < 10.5$, Isoc. method | — | — | 2012AJ...144..185C |
| | | -0.125 ± 0.008 | $7 < R_{gc} < 10.5$, Photo. method | — | — | 2012AJ...144..185C |
| Bilir et al. (2012) | RCs | — | — | -0.109 ± 0.008 | $TD/D \leq 0.1$ | 2012MNRAS.421.3362B |
| | | — | — | -0.260 ± 0.031 | $e_v \leq 0.07$ | 2012MNRAS.421.3362B |
| | | — | — | -0.167 ± 0.011 | $e_v \leq 0.12$ | 2012MNRAS.421.3362B |
| | | — | — | -0.022 ± 0.005 | $e_v > 0.25$ | 2012MNRAS.421.3362B |
| Peng et al. (2012) | MSs | -0.210 ± 0.050 | $0 < Z < 2$ | — | — | 2012MNRAS.422.2756P |
| Katz et al. (2011) | RGB,RCs,HB,MS,SG | -0.068 ± 0.009 | Thick disc | — | — | 2011A&A...525A..90K |
| Chen et al. (2011) | RHB | -0.120 ± 0.010 | $0.5 < Z < 3$ | — | — | 2011AJ...142..184C |
| | | -0.220 ± 0.070 | $1 < Z < 3$ | — | — | 2011AJ...142..184C |
| Kordopatis et al. (2011) | FGK MSs | -0.140 ± 0.050 | $1 \leq Z \leq 4$ | — | — | 2011A&A...535A.107K |
| Ruchti et al. (2011) | RGB,RCs,HB,MS,SG | -0.090 ± 0.050 | $6 < R_{gc} < 10$, $ Z < 3$ | — | — | 2011ApJ...737...9R |
| Yaz & Karaali (2010) | G MSs | -0.320 ± 0.010 | $Z < 2.5$ | — | — | 2010NewA...15..234Y |
| | | -0.300 ± 0.060 | $3 < Z < 5.5$ | — | — | 2010NewA...15..234Y |
| | | -0.010 ± 0.010 | $6 < Z < 10$ | — | — | 2010NewA...15..234Y |
| Siegel et al. (2009) | FS | -0.150 | $Z < 4$ | — | — | 2009MNRAS.395.1569S |
| Soubiran et al. (2008) | RCs | -0.300 ± 0.030 | $d < 1$ | — | — | 2008A&A...480...91S |
| | | — | — | -0.310 ± 0.060 | $0 \leq z_{max} < 1.2$ | 2008A&A...480...91S |
| Ak et al. (2007a) | G MSs | -0.380 ± 0.060 | $3 \leq Z < 5$ | — | — | 2007NewA...12..605A |
| | | -0.080 ± 0.070 | $5 \leq Z < 10$ | — | — | 2007NewA...12..605A |
| Ak et al. (2007b) | G MSs | -0.160 ± 0.020 | $Z < 3$ North | — | — | 2007AN...328..169A |
| | | -0.220 ± 0.020 | $Z < 3$ South | — | — | 2007AN...328..169A |
| Allende Prieto et al. (2006) | FG MSs | 0.030 | $1 < Z \leq 3$; $[Fe/H] > -1.2$ | — | — | 2006ApJ...636..804A |
| Marsakov & Borkova (2006) | FS | -0.290 ± 0.060 | Thin disc | — | — | 2006A&AT...25..157M |
| Chen et al. (2003) | OC | — | — | -0.295 ± 0.050 | $6 < R_{gc} < 15$ | 2003AJ...125.1397C |
| Karaali et al. (2003) | G MSs | -0.200 | $Z \leq 8$ | — | — | 2003MNRAS.343.1013K |
| Bartašiūtė et al. (2003) | FS | -0.230 ± 0.040 | $Z < 1.3$ | — | — | 2003BaltA...12..539B |

Abbreviations: Main Sequence Stars: MSs; Red Clump Stars: RCs; Red Giants: RG; Open Cluster: OC; Red Giant Branch: RGB; Horizontal Branch: HB; Red Horizontal Branch: RHB;

Sub-giant: SG; Field Stars: FS.

2 The Data

The data are selected from the Radial Velocity Experiment's fourth data release (DR4; Kordopatis et al., 2013). RAVE DR4 is the first RAVE release that uses DENIS *I*-band magnitude for its input catalogue, instead of pseudo *I*-band magnitude. The new catalogue presents radial velocities for 482,430 stars. The internal errors in radial velocities are reduced from ~ 2 km s⁻¹ to 1.4 km s⁻¹ for 68% of the RAVE DR4 sample in comparison with 68% of the RAVE DR3 sample (Siebert et al., 2011). Radial velocity errors of the sample have median value at 0.80 ± 0.24 km s⁻¹. One of the important features of this data release is that it uses a new pipeline with MATISSE (Recio-Blanco et al., 2006) and DEGAS (Bijaoui et al., 2012) algorithms to derive more reliable stellar atmospheric parameters (effective temperature, surface gravity, and metallicity), where Kordopatis et al. (2013) extends the grid used in Bijaoui et al. (2012) from 4500 K down to 3000 K. Also, the proper motions of stars combined from various source catalogues such as Tycho-2 (Hog et al., 2000), UCAC2, UCAC3, UCAC4 (Zacharias et al., 2010, 2013), PPMX, PPMXL (Roeser et al., 2010) and SPM4 (Girard et al., 2011), all of which covers different portions of sample stars. UCAC4 proper motions are selected as an input for kinematic parameter calculations since it covers 98% of the RAVE DR4 data. Proper motion errors range from 0.5 to 4 mas yr⁻¹ and its median value is 1.69 ± 0.65 mas yr⁻¹. The near infrared magnitudes are taken from the Two Micron All Sky Survey (2MASS; Skrutskie et al., 2006), All-Sky Catalog of Point Sources (2MASS; Cutri et al., 2003).

Distances of the RAVE DR4 stars were estimated by two different procedures. One is from Zwitter et al. (2010)'s method of projection of individual stellar parameters from RAVE DR4 pipelines on a set of isochrones and obtains the most likely value for a star's absolute magnitudes. The other is from Binney et al. (2014)'s Bayesian distance-finding method, which is an improved version of Burnett & Binney (2010)'s algorithm. However, in our study the distances for our RC sample are calculated by a different procedure. In distance estimation of the RC stars we preferred near infrared magnitudes of 2MASS. These photometric bands are not affected much from interstellar reddening and absorption. The K_s absolute magnitude of the RC stars only has a weak dependence on metallicity. This relation demonstrated in many studies within the last decade (see for example Lopez-Corredoira et al., 2002, 2004; Cabrera-Lavers et al., 2005, 2007a,b, 2008; Bilir et al., 2012, and references therein).

In Fig. 1, $T_{\text{eff}} - \log g$ diagram of the region where the RC stars most likely to reside are presented as colour coded diagrams in two panels, one with logarithmic number density and the other with logarithmic

metallicity. Also, 1σ and 2σ contour lines based on the most crowded region are drawn on the figure. Depending on the contour lines, we selected the stars that reside in the 1σ area which correspond to 68,663 stars. The whole region covers $1 < \log g < 3$ and $4000 < T_{\text{eff}}(K) < 5400$. Selection of suitable RC sample also depends on other constraints: (1) having a cross matched UCAC4 catalogue (Zacharias et al., 2013) proper motion values (since it covers the largest portion of the sample compared with other proper motion catalogues); (2) having metallicity values from the RAVE DR4 chemical pipeline (Kordopatis et al., 2013); (3) according to Kordopatis et al. (2013), stars with $S/N \geq 40$ in the RAVE DR4 catalogue have more accurate astrophysical parameters so this cut was made; (4) avoid repeated observations. This reduces the number of stars to 52,196.

Given that Fig. 1 is a pseudo-HR diagram, it shows that stars on the first ascent of the giant branch have brighter absolute magnitudes as $\log g$ and T_{eff} both decrease. Brighter absolute magnitudes correspond to larger line-of-sight distances. As RAVE observes away from the Galactic plane, larger line-of-sight distances means statistically larger numbers of thick disc stars and thus lower metallicities. Fig. 2 shows there is a correlation between $[\text{Fe}/\text{H}]$ and T_{eff} and between $[\text{Fe}/\text{H}]$ and $\log g$ in our RC sample, which suggests it is contaminated with first ascent giants. With a similar selection of RC stars, Williams et al. (2013) showed that the first ascent giants in their RC sample have a very similar distance distribution. Given this and that there is also a real dispersion in absolute magnitude among bona fide RC stars, such distance uncertainties will reduce our measured gradients. Nevertheless as we looking for general trends, we consider such an effect to be second order.

We adopted Groenewegen (2008)'s $M_{K_s} = -1.54 \pm 0.04$ mag for the sample. Using Schlafly & Finkbeiner (2011)'s reddening maps, we evaluated the $E_{\infty}(B - V)$ colour excess for each star individually, and obtained the reduced value of colour excess $E_d(B - V)$ related to their respective distances of each star in the RC sample by using Bahcall & Soneira (1980)'s equation. Further iterations were carried out for the dereddening of the K_s apparent magnitude for each star (cf. Coşkunoğlu et al., 2011, 2012). In Fig. 3, panels (a) and (b) represent the original colour excess ($E_{\infty}(B - V)$) and the reduced colour excess $E_d(B - V)$ of the RC stars as colour coded in Galactic coordinates, respectively.

The distance histogram of the sample stars is presented in Fig. 4. The median distance and its standard deviation are $d = 1$ and $\sigma = 0.37$ kpc, respectively. The median value for the relative distance errors is 0.05 kpc. Heliocentric space distributions of the RC stars are shown in Fig. 5 in two panels. Most of the stars are found in the first and fourth Galactic quadrants. The median distance values of the sample in X , Y

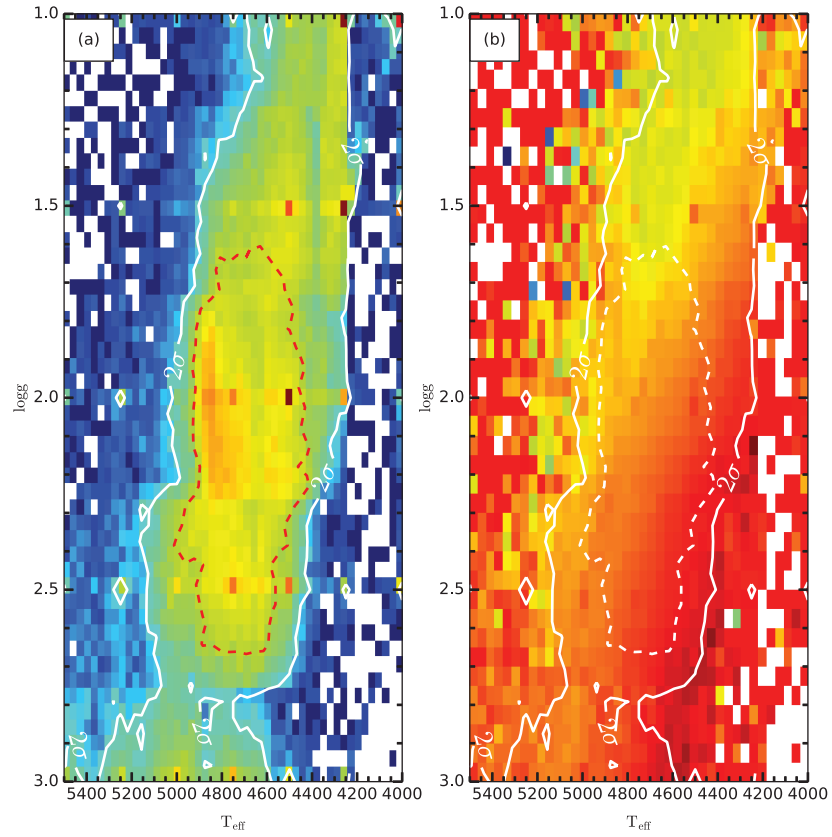


Figure 1. $T_{\text{eff}} - \log g$ diagram of the RC region, colour coded for logarithmic number density (a). Red dashed and white solid lines show 1σ and 2σ regions, respectively. $T_{\text{eff}} - \log g$ diagram of the RC region, colour coded for metallicity (b). White dashed and solid lines show 1 and 2σ regions, respectively.

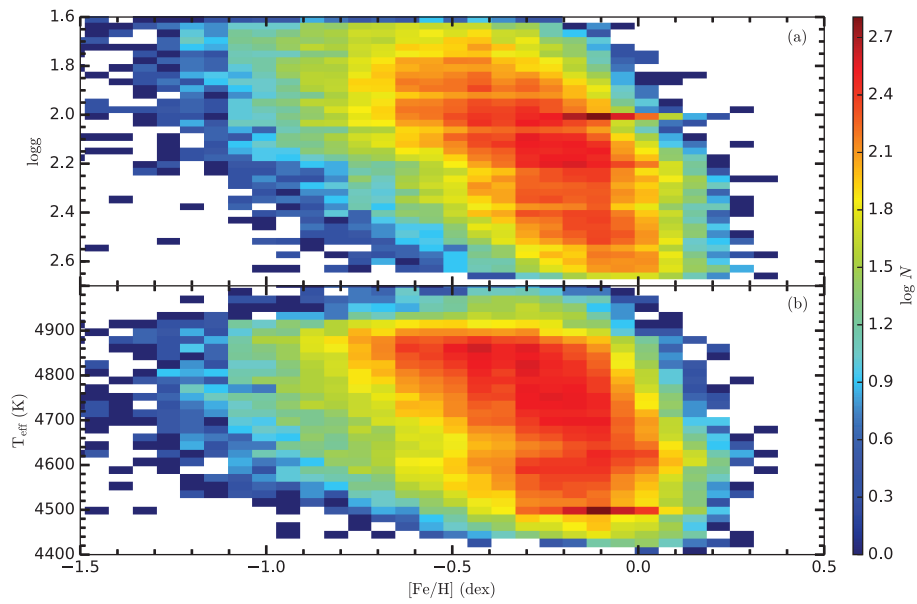


Figure 2. $T_{\text{eff}} - [\text{Fe}/\text{H}]$ and $\log g - [\text{Fe}/\text{H}]$ diagram of our RC sample.

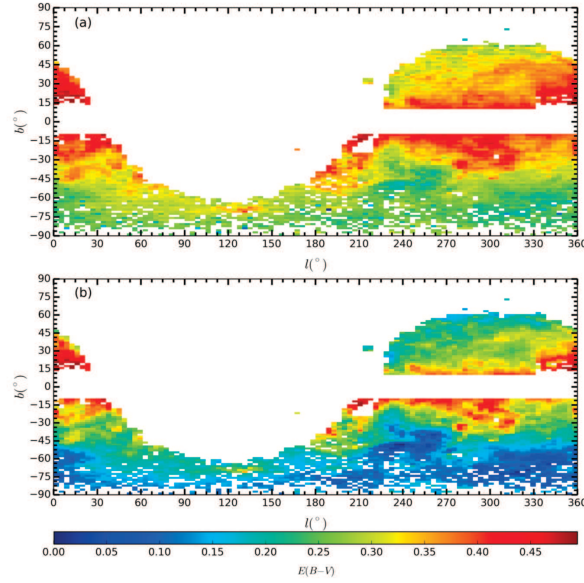


Figure 3. Colour coded for $E_{\infty}(B - V)$ colour excess (a), and reduced colour excess $E_d(B - V)$ (b) distributions of 52,196 stars in Galactic coordinates.

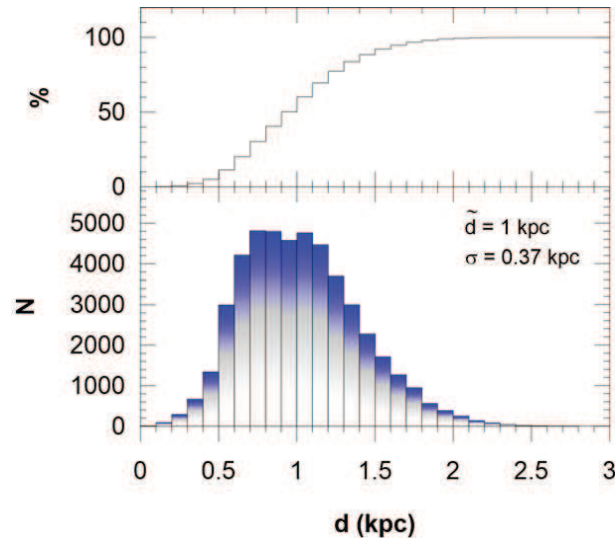


Figure 4. Distance histogram of 52,196 the RC stars. Median and standard deviation of distance distribution are 1 and 0.37 kpc, respectively. The corresponding percentage of RC stars are also shown in the upper panel of the diagram.

and Z are 0.67, 0.09, and -0.24 kpc, respectively. Our sample covers a distance range of $0 < |Z| < 3$ kpc and $5.5 < R_{gc} < 11$ kpc. However, most of our sample stars (83.6%) are concentrated in $7 < R_g < 9$ kpc.

RAVE DR4 line-of-sight velocities (Kordopatis et al., 2013), UCAC4 proper motions (Zacharias et al., 2013) and photometric distances are combined to obtain space velocity components (U , V , W) of 52,196 RC stars, which are calculated with Johnson & Soderblom (1987)'s standard algorithms and the transformation matrices of a right handed system for epoch J2000 (as described in the International Celestial Reference Sys-

tem of the *Hipparcos* and *Tycho-2* Catalogues (ESA, 1997). Hence, U , V and W are the components of a velocity vector of a star with respect to the Sun, where U is positive towards the Galactic centre ($l = 0^\circ$, $b = 0^\circ$), V is positive in the direction of Galactic rotation ($l = 90^\circ$, $b = 0^\circ$) and W is positive towards the North Galactic Pole ($b = 90^\circ$). The Galactic rotational velocity of the Sun is adopted as 222.5 km s^{-1} (Schönrich, 2012). Since stars in our Galaxy orbit around the Galactic center with different speeds, Mihalas & Binney (1981) suggested a series of corrections on U and V space velocities in order to compen-

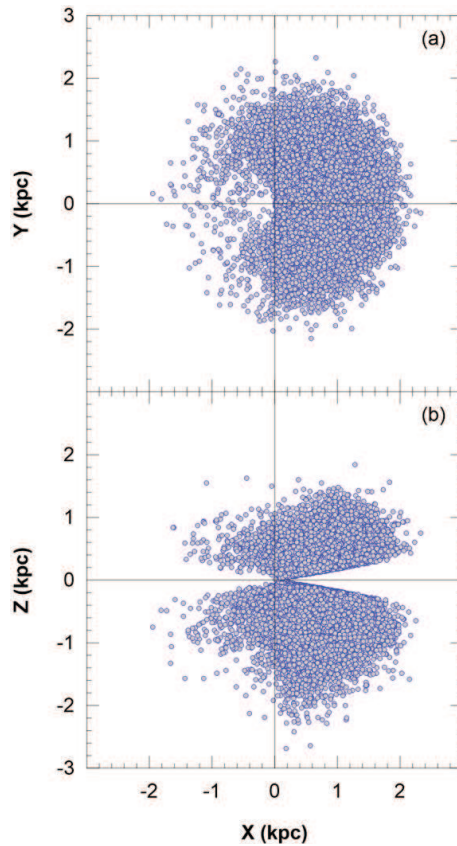


Figure 5. Heliocentric distribution of the RC stars projected on X - Y and X - Z planes.

sate for this. The W space velocity is not affected by this behavior thus needed no correction. The first order Galactic differential rotation corrections are $-61.29 < dU < 34.12$ and $-3.76 < dV < 5.34$ km s^{-1} . Then, space velocities are reduced by applying solar local standard of rest values (LSR) of Coşkunoğlu et al. (2011) for all stars $(U_{\odot}, V_{\odot}, W_{\odot})_{\text{LSR}} = (8.83 \pm 0.24, 14.19 \pm 0.34, 6.57 \pm 0.21)$ km s^{-1} to LSR.

Using Johnson & Soderblom (1987)'s algorithm, the uncertainties of space velocities are calculated by propagating the uncertainties in radial velocity, proper motion and distance. Kinematic input parameter errors vary in $0.3 < \gamma < 6.6$ km s^{-1} , $0.5 < \mu < 7$ mas yr^{-1} , and $0.01 < \sigma_{\pi}/\pi < 0.13$ intervals for radial velocity, proper motion and distance, respectively and their corresponding medians and standard deviations are 0.80 ± 0.24 , 1.69 ± 0.65 and 0.05 ± 0.26 , respectively. The total space velocity errors are calculated as a square root of individual space velocity errors of the RC stars, i.e. $(S_{err}^2 = U_{err}^2 + V_{err}^2 + W_{err}^2)$. The distribution of total space velocities of 52,196 RC stars is presented in Fig. 6a. We applied a final constraint on total space velocity errors of the RC stars. In order to remove the most discrepant stars, we applied a cut-off point of 21 km s^{-1} which is deduced from the stars within 1 -

σ prediction in total space velocity error. Thus, our final sample is reduced to 47,406 RC stars. The final sample has the median space velocity errors and standard deviations of $(U_{err}, V_{err}, W_{err}) = (-4.92 \pm 2.86, 4.03 \pm 2.94, 4.88 \pm 2.85)$ km s^{-1} . In Fig. 6b-d the histograms of space velocity errors for the final RC sample are shown. Figs. 7 and 8 show the space velocity and metallicity distributions of the final RC sample respectively. Using Johnson & Soderblom (1987)'s algorithm, the uncertainties of space velocities are calculated by propagating the uncertainties in radial velocity, proper motion and distance. Kinematic input parameter errors vary in $0.3 < \gamma < 6.6$ km s^{-1} , $0.5 < \mu < 7$ mas yr^{-1} , and $0.01 < \sigma_{\pi}/\pi < 0.13$ intervals for radial velocity, proper motion and distance, respectively and their corresponding medians and standard deviations are 0.80 ± 0.24 , 1.69 ± 0.65 and 0.05 ± 0.26 , respectively. The total space velocity errors are calculated as a square root of individual space velocity errors of the RC stars, i.e. $(S_{err}^2 = U_{err}^2 + V_{err}^2 + W_{err}^2)$. The distribution of total space velocities of 52,196 RC stars is presented in Fig. 6a. We applied a final constraint on total space velocity errors of the RC stars. In order to remove the most discrepant stars, we applied a cut-off point of 21 km s^{-1} which is deduced from the stars within 1 - σ pre-

diction in total space velocity error. Thus, our final sample is reduced to 47,406 RC stars. The final sample has the median space velocity errors and standard deviations of $(U_{err}, V_{err}, W_{err}) = (-4.92 \pm 2.86, 4.03 \pm 2.94, 4.88 \pm 2.85)$ km s⁻¹. In Fig. 6b-d the histograms of space velocity errors for the final RC sample are shown. Figs. 7 and 8 show the space velocity and metallicity distributions of the final RC sample respectively.

Binney et al. (2014) find that their absolute magnitudes peak at $M_{K_s} = -1.53$ mag (see their Fig. 10). As we have used an almost identical value with them ($M_{K_s} = -1.54 \pm 0.04$ mag), we expect our distances to be very similar to the Binney et al. (2014) distances. Fig. 9 compares the distances of our final RC sample to the Binney et al. (2014)'s in RAVE DR4. While Fig. 9 shows that the Binney et al. (2014) distances are systematically larger, they are still, as expected very similar: the mean and standard deviation of the distance difference between the two methods is 87 pc and 220 pc respectively. Out of our 47,406 RC stars, RAVE DR4-Binney et al. (2014) provides distances to 41,221 i.e. it is missing 13% of the sample. Given that our distances are very similar to the Binney et al. (2014) distances and provide a larger sample, we have used our photometric parallax estimation for our metallicity gradient analysis.

Dynamical properties of individual stars in the RC sample are calculated via *MWPotential2014* model in *galpy* Galactic dynamics library of Bovy (2015), which is given in detail in Table 1 of his paper. Test-particle integration for the combined Milky Way potential (for bulge, disc and halo) over 3 Gyrs is performed to obtain the Galactic orbital parameters of the closed orbit for a given star. Celestial equatorial coordinates, distances, proper motions and radial velocities of our stars are used as input parameters in the calculations of the Galactic orbital parameters such as apogalactic and perigalactic distances, maximum vertical distance from the Galactic plane, orbital angular momenta and eccentricities are obtained as output parameters.

Gradient analysis are performed both for the current orbital status of the stars and for their complete orbits. Thus, various radial and vertical distances are considered in calculations such as current Galactocentric distance (R_{gc}), current absolute vertical distance from the Galactic plane ($|Z|$), mean Galactocentric distance (R_m), which is the arithmetic mean of the perigalactic (r_p) and apogalactic (r_a) distances of a star's orbit, and maximum vertical distances from the Galactic plane towards the North (z_{max}) and South Galactic (z_{min}) poles of a star's entire orbit. Moreover, general distribution of stars on the planar and vertical eccentricity planes are investigated. Planar eccentricity is an output from the *galpy* dynamical library ($e_p = \frac{r_a - r_p}{r_a + r_p}$), while vertical eccentricities are calculated as $e_v = \frac{\frac{1}{2}(|z_{max}| + |z_{min}|)}{R_m}$.

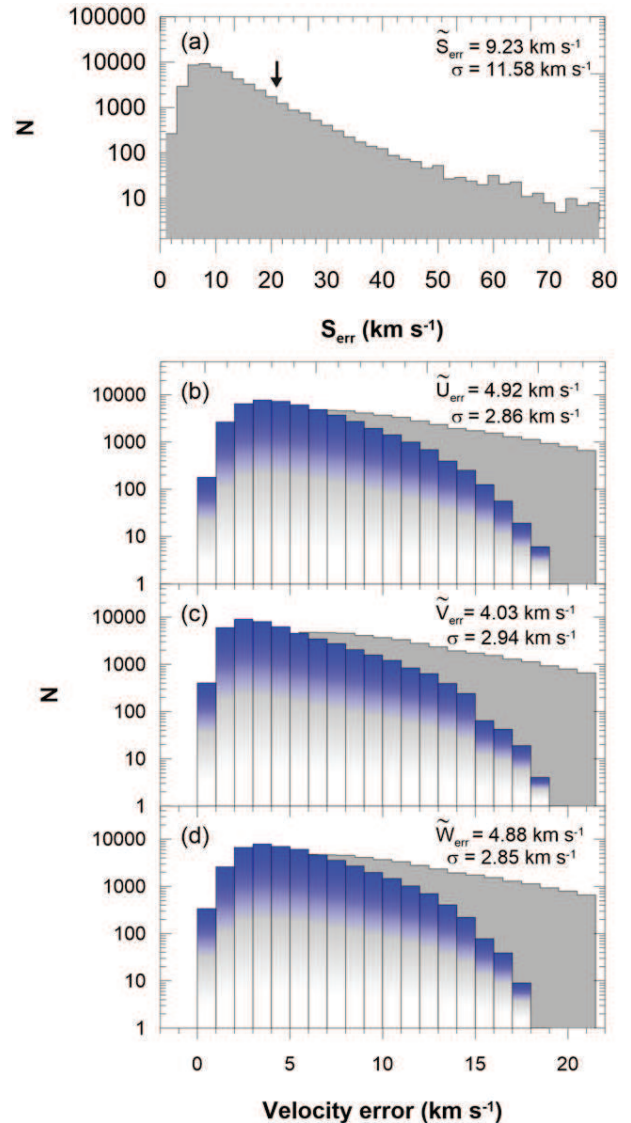


Figure 6. Total space velocity error histogram of 52,196 stars (*top panel*). The median and standard deviation are 9.23 km s⁻¹ and 11.58 km s⁻¹, respectively, which of their sum gives approximately 21 km s⁻¹ and this is the last constraint that applied to the sample. As a result 47,406 RC stars are remained as the final sample. Histograms of U , V , and W space velocity errors in comparison with total space velocity error histogram of 47,406 RC stars (*lower panels*).

3 Results

The metallicity gradients of our RC stars are considered in two general regimes: one for their current orbital positions and one from orbital properties calculated for 3 Gyrs with 2 Myr steps, which give stars to have enough time to close their orbits. In order to calculate metallicity gradients, linear fits are applied to the data for each selected sub-sample.

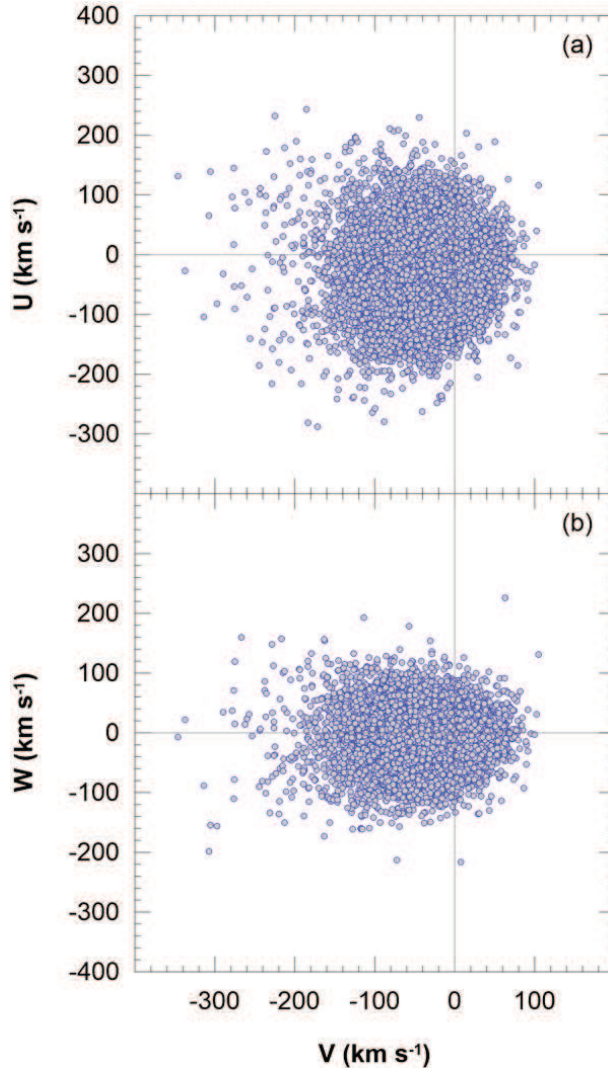


Figure 7. Distribution of space velocity components of the RC stars in V - U and V - W planes.

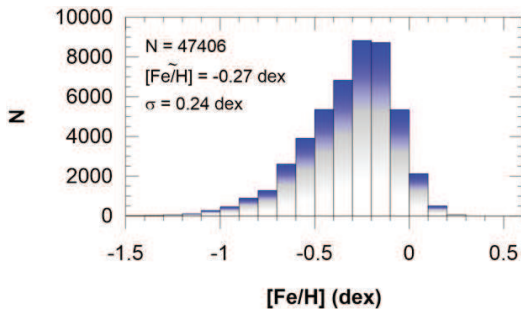


Figure 8. Metallicity histogram of 47,406 RC stars. Median metallicity of the distribution is $[\text{Fe}/\text{H}] = -0.27$ dex and its standard deviation $\sigma_{[\text{Fe}/\text{H}]} = 0.24$ dex.

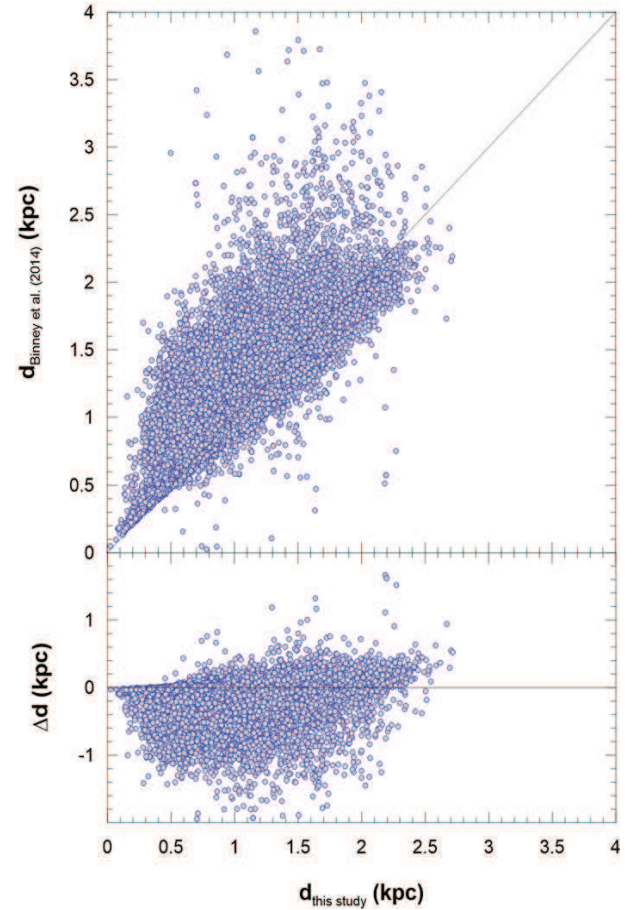


Figure 9. Distance comparison of this study and Binney et al. (2014).

3.1 Metallicity Gradients from the Current Positions of the Stars

Even though RAVE is a shallow sky survey ($9 < I < 13$), RC stars have such bright absolute magnitudes ($M_{K_s} = -1.54$ mag) that these stars reach up to 3 kpc distance from the Sun in our sample (see Fig. 3). Thus, calculations of radial and vertical metallicity gradients are applicable from their current positions in the Galaxy.

In order to calculate radial metallicity gradients of the final RC star sample, the relation between R_{gc} and $[\text{Fe}/\text{H}]$ are analyzed for three $|Z|$ intervals, i.e. $0 \leq |Z| \leq 0.5$, $0.5 < |Z| \leq 1$, and $1 < |Z| < 3$ kpc. The resulting gradients are listed in Table 3 and shown in Fig. 10. Radial metallicity gradients vary from -0.047 ± 0.003 to $+0.015 \pm 0.008$ dex kpc^{-1} with increasing $|Z|$ intervals. A similar trend is also seen in median metallicities of the sub-samples, which also vary from -0.26 to -0.42 dex in Table 3 (column 3). These results show that the radial gradients become flatter as the $|Z|$ distances become larger which is an expected result because as $|Z|$ increases more and more stars are members of the thick disc, which presents no radial metallicity gradient.

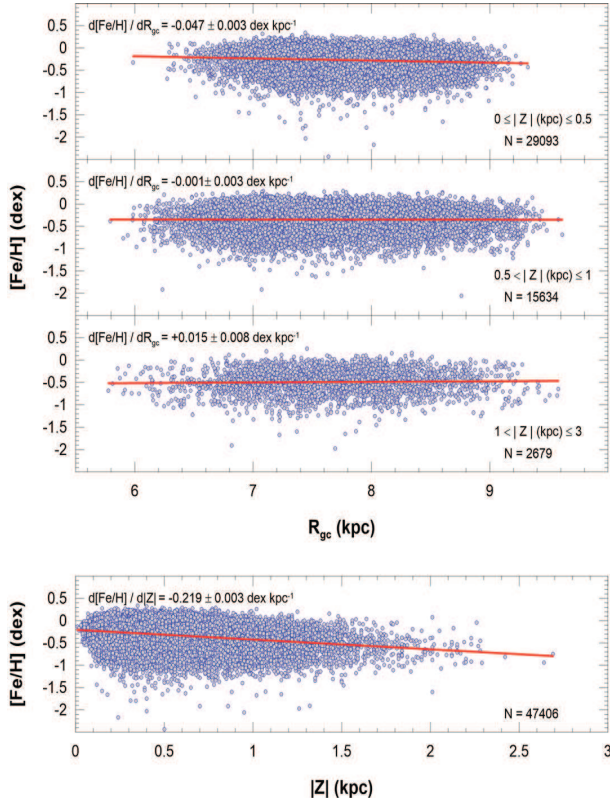


Figure 10. Radial metallicity gradients for current Galactocentric distance of 47,406 RC stars in three $|Z|$ intervals, i.e. $0 \leq |Z| \leq 0.5$, $0.5 < |Z| \leq 1$, and $1 < |Z| \leq 3$ kpc (*upper panels*). Vertical metallicity gradients for current distance from the Galactic plane of the same sample (*lower panel*).

Analogously, vertical metallicity gradients that are obtained from the relation between $|Z|$ and $[\text{Fe}/\text{H}]$ of the RC star sample is presented in Fig. 10 (lower panel), and it's resulting value is -0.219 ± 0.003 dex kpc^{-1} , which shows that there is a significant vertical metallicity gradient within the Galactic disc in $0 < |Z| < 3$ kpc distance interval.

Table 3 Radial metallicity gradients of the RC stars in each Z interval for current orbital positions.

| $ Z $ interval (kpc) | N | $\langle [\text{Fe}/\text{H}] \rangle$ (dex) | $d[\text{Fe}/\text{H}]/dR_{gc}$ (dex kpc^{-1}) |
|----------------------|-------|--|--|
| 0.0-0.5 | 29093 | -0.26 | -0.047 ± 0.003 |
| 0.5-1.0 | 15635 | -0.29 | -0.003 ± 0.001 |
| 1.0-3.0 | 2678 | -0.42 | $+0.015 \pm 0.008$ |

3.2 Metallicity Gradients from the Galactic Orbits of Stars

Galactic orbital parameters of the RC stars are used in order to obtain R_m and z_{max} of a given star. Then, radial and vertical gradients are calculated as func-

tions of these parameters accordingly. The resulting values of the radial metallicity gradient are listed in Table 4 and shown in Fig. 11 for four z_{max} intervals, i.e. $0 \leq z_{max} \leq 0.5$, $0.5 < z_{max} \leq 1$, $1 < z_{max} \leq 2$, and $z_{max} > 2$ kpc. Overall radial gradients change between -0.025 ± 0.002 and $+0.030 \pm 0.004$ dex kpc^{-1} . Similarly median metallicities of the sub-samples vary from -0.22 to -0.57 dex with increasing z_{max} in Table 4 (column 3). Sign of the gradients change from negative to positive for $z_{max} > 1$ kpc which is generally considered as the domain of thick-disc stars where no or positive gradients are expected. According to Jurić et al. (2008), $Z = 1$ kpc is the transition region where the thin-disc component loses density in the number of stars and the thick-disc population becomes dominant.

Table 4 Radial metallicity gradients of the RC stars in each z_{max} interval for complete stellar orbits.

| z_{max} interval (kpc) | N | $\langle [\text{Fe}/\text{H}] \rangle$ (dex) | $d[\text{Fe}/\text{H}]/dR_m$ (dex kpc^{-1}) |
|--------------------------|-------|--|---|
| 0-0.5 | 17401 | -0.22 | -0.025 ± 0.002 |
| 0.5-1 | 19243 | -0.27 | -0.003 ± 0.001 |
| 1-2 | 8935 | -0.39 | $+0.024 \pm 0.002$ |
| >2 | 1827 | -0.57 | $+0.030 \pm 0.004$ |

Although the z_{max} distances of the RC stars can be as large as 16 kpc in the sample, 99% of them lie within $z_{max} \leq 3$ kpc interval. Hence, we evaluated the vertical metallicity gradients for this range. Our result, -0.157 ± 0.002 dex kpc^{-1} , indicates a steep metallicity gradient in the vertical direction for the Galactic disc. However, the metallicity gradient that is obtained for $|Z|$ distances in Section 3.1 is steeper than the one obtained for z_{max} , i.e. -0.219 ± 0.003 dex kpc^{-1} .

3.3 Metallicity Gradients According to Eccentricities and Their Implications

Instead of assigning populations to the RC stars with any known methods, i.e. dynamical, chemical or statistical, we considered the Galactic disc as a whole and see how the stellar properties such as metallicity, space velocities, eccentricity, orbital angular momenta etc., vary with distance. Variations in metallicity gradients are examined with an additional constraint, i.e. the orbital eccentricities, to the aforementioned z_{max} intervals.

3.3.1 Radial Metallicity Gradients

Table 5 and Fig. 12 give the radial metallicity gradients that we found for four z_{max} intervals. As e_p values increase from 0.05 to 0.20 in the $0 \leq z_{max} \leq 0.5$ kpc distance interval, the radial metallicity gradients vary between -0.089 ± 0.010 and -0.044 ± 0.002 dex kpc^{-1} , respectively. Unlike the first z_{max} interval, radial metallicity gradients tend to remain around the same e_p lim-

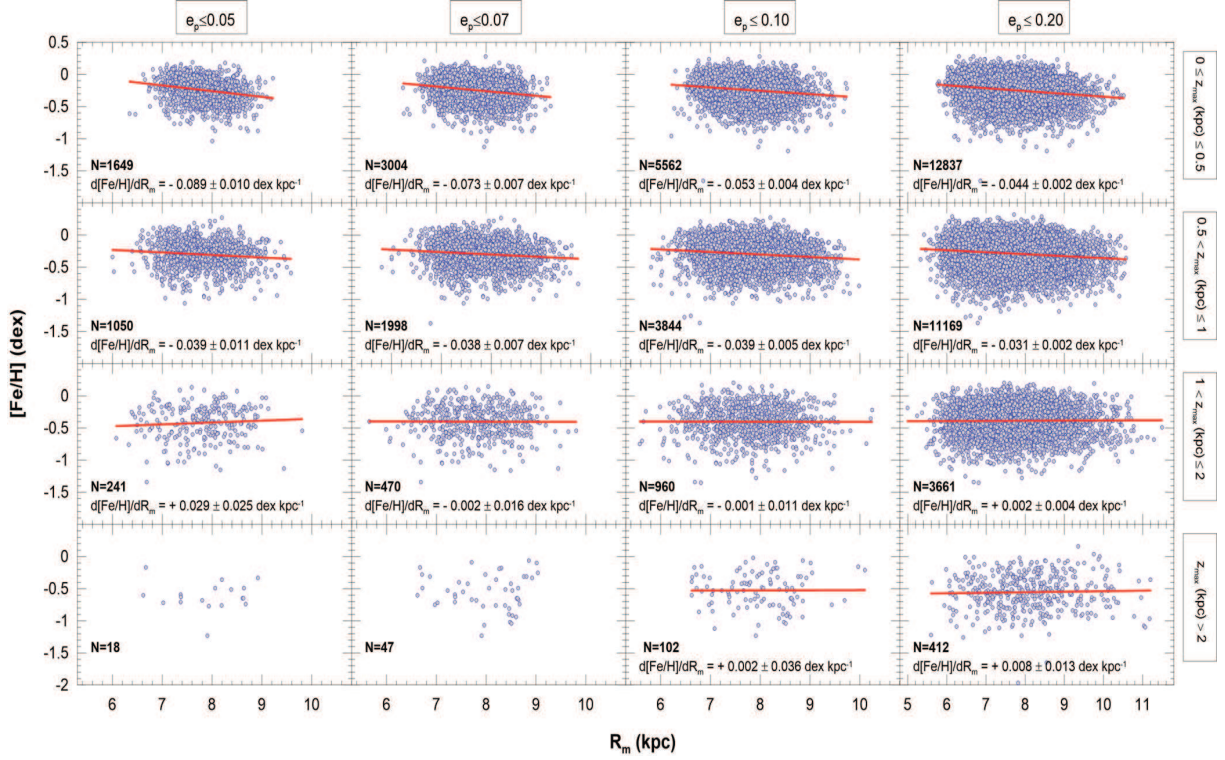


Figure 12. Radial metallicity gradients for R_m of 47,406 RC stars for consecutive e_p sub-samples, i.e. $e_p \leq 0.05$, $e_p \leq 0.07$, $e_p \leq 0.10$ and $e_p \leq 0.20$, in four z_{max} intervals. Metallicity gradients and number of stars in each corresponding interval are also shown in the panels.

Table 5 Radial metallicity gradients of the RC stars for consecutive e_p limits, i.e. ≤ 0.05 , 0.07 , 0.10 and 0.20 , in each z_{max} intervals.

| z_{max} interval (kpc) | $e_p \leq 0.05$ | | | $e_p \leq 0.07$ | | |
|-----------------------------|-----------------|-----------------------------------|--------------------------------------|-----------------|-----------------------------------|--------------------------------------|
| | N | $\langle [Fe/H] \rangle$ (dex) | $d[Fe/H]/dR_m$ (dex kpc $^{-1}$) | N | $\langle [Fe/H] \rangle$ (dex) | $d[Fe/H]/dR_m$ (dex kpc $^{-1}$) |
| 0-0.5 | 1649 | -0.23 | -0.089 ± 0.010 | 3004 | -0.23 | -0.073 ± 0.007 |
| 0.5-1 | 1050 | -0.28 | -0.039 ± 0.011 | 1998 | -0.27 | -0.038 ± 0.007 |
| 1-2 | 241 | -0.39 | $+0.029 \pm 0.025$ | 470 | -0.39 | -0.002 ± 0.016 |
| > 2 | 18 | – | – | 47 | – | – |
| z_{max} interval (kpc) | $e_p \leq 0.10$ | | | $e_p \leq 0.20$ | | |
| | N | $\langle [Fe/H] \rangle$ (dex) | $d[Fe/H]/dR_m$ (dex kpc $^{-1}$) | N | $\langle [Fe/H] \rangle$ (dex) | $d[Fe/H]/dR_m$ (dex kpc $^{-1}$) |
| 0-0.5 | 5562 | -0.23 | -0.053 ± 0.004 | 12837 | -0.22 | -0.044 ± 0.002 |
| 0.5-1 | 3844 | -0.27 | -0.039 ± 0.005 | 11169 | -0.26 | -0.031 ± 0.002 |
| 1-2 | 960 | -0.40 | -0.001 ± 0.011 | 3661 | -0.37 | $+0.002 \pm 0.004$ |
| > 2 | 102 | -0.52 | $+0.020 \pm 0.036$ | 412 | -0.55 | $+0.008 \pm 0.013$ |

itation for $0.5 < z_{max} \leq 1$ kpc interval. In the remaining z_{max} distance intervals, $1 < z_{max} \leq 2$ and $z_{max} > 2$ kpc, the radial gradients show no trends. However, when all the RC stars in $0 \leq z_{max} \leq 0.5$ kpc interval are considered, the radial gradient slope becomes -0.025 ± 0.002 dex kpc $^{-1}$.

In Fig. 13, planar versus vertical eccentricity distribution of 47,406 RC stars are plotted in four z_{max} intervals, i.e. $0 \leq z_{max} \leq 0.5$, $0.5 < z_{max} \leq 1$, $1 < z_{max} \leq 2$,

and $z_{max} > 2$ kpc. The median value of eccentricities change from 0.14 to 0.43 in e_p as higher z_{max} intervals are considered. Young thin disc stars are predominately on circular orbits (e_p close to 0) with z_{max} close to the Galactic plane. Older thin disc stars have slightly higher e_p and z_{max} . Thick disc stars in RAVE have an asymmetric peak at $e_p = 0.2$ with a relatively smooth falloff towards higher eccentricities (Wilson et al., 2011). Therefore the closest z_{max} inter-

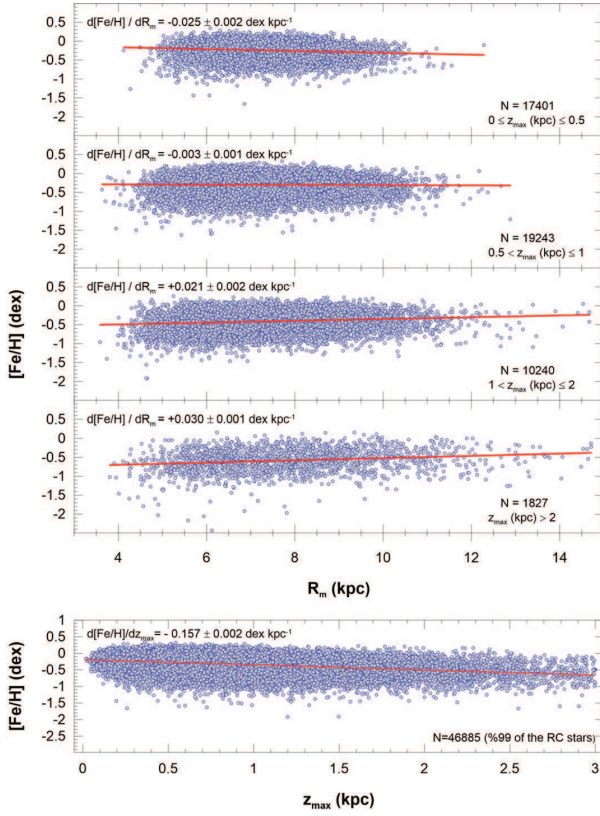


Figure 11. Radial metallicity gradients for mean Galactocentric distances of 47,406 RC stars in four z_{max} intervals, i.e. $0 \leq z_{max} \leq 0.5$, $0.5 < z_{max} \leq 1$, $1 < z_{max} \leq 2$, and $z_{max} > 2$ kpc (*upper panels*). Vertical metallicity gradient for maximum distance from the Galactic plane of the same sample (*lower panel*).

val to the Galactic plane is dominated by thin disc stars. As the z_{max} interval increases, the ratio of the thin disc stars to thick disc stars decreases, so e_p also increases. The median value of eccentricities change from 0.09 to 0.68 in e_v as higher z_{max} intervals are considered. This is because e_v is proportional to z_{max} by definition.

In Tables 3 and 4, the radial metallicity gradient in the interval of 0.5-1 kpc interval from the plane is essentially flat. However, when this same interval is limited to low e_p , there is a negative gradient that remains the same when including more and more higher e_p stars. This suggests that stars with $e_p > 0.2$ have positive gradients so they cancel out the negative gradients of stars with $e_p < 0.2$.

3.3.2 Vertical Metallicity Gradients

Vertical metallicity gradients of RC stars for four e_p sub-samples are calculated regardless of z_{max} intervals and shown in Table 6 and Fig. 14. Gradient values change between -0.175 ± 0.007 and -0.144 ± 0.002 dex kpc^{-1} and so get shallower as e_p increases from 0.05 to 0.20. Mikolaitis et al. (2014) found that their vertical metallicity gradient becomes shallower going from their

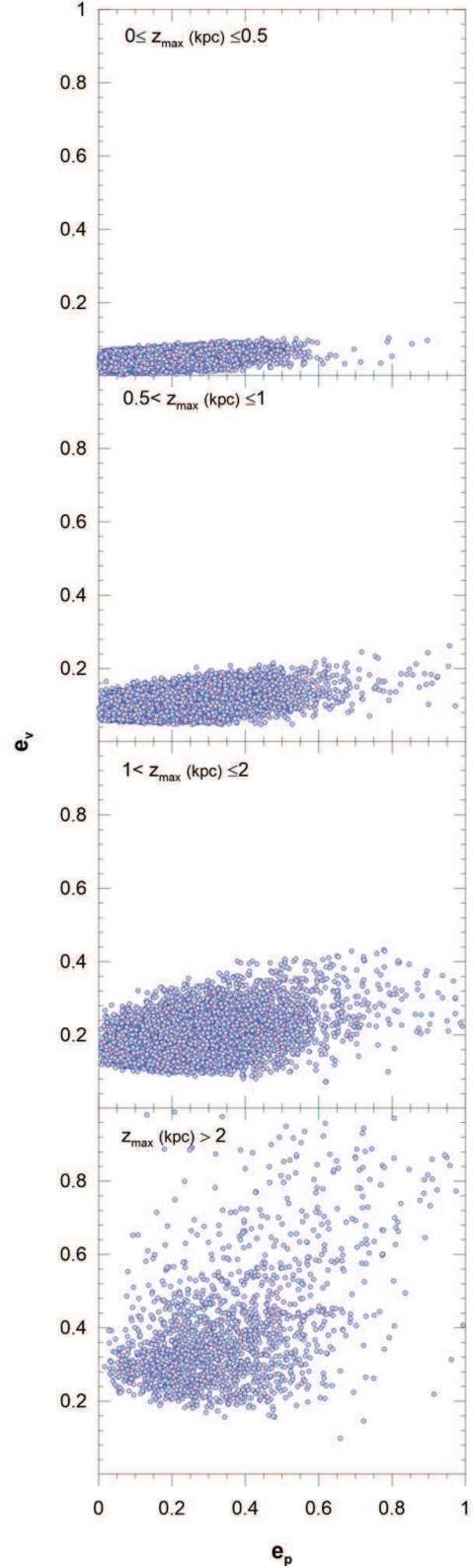


Figure 13. $e_p - e_v$ diagram of the RC stars for four z_{max} intervals.

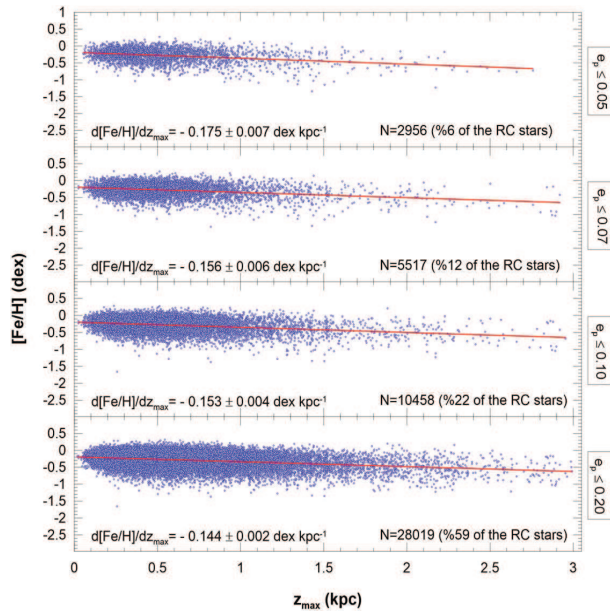


Figure 14. Vertical metallicity gradients for z_{max} of 47,406 RC stars for consecutive e_p sub-samples, i.e. $e_p \leq 0.05$, $e_p \leq 0.07$, $e_p \leq 0.10$ and $e_p \leq 0.20$. Metallicity gradients and number of stars in each corresponding interval are also shown in the panels.

thin disc sample to their thick disc sample. Given that thick disc stars are generally more eccentric than thin disc stars, our e_p cut progressively lets in more thick disc stars and so is consistent with Mikolaitis et al. (2014).

Table 6 Vertical metallicity gradients of the RC stars for consecutive e_p limits, i.e. ≤ 0.05 , 0.07, 0.10 and 0.20, in $0 < z_{max} \leq 3$ kpc interval.

| e_p range | N | $d[\text{Fe}/\text{H}]/dz_{max}$ (dex kpc $^{-1}$) |
|-----------------|-------|--|
| $e_p \leq 0.05$ | 2956 | -0.175 ± 0.007 |
| $e_p \leq 0.07$ | 5517 | -0.156 ± 0.006 |
| $e_p \leq 0.10$ | 10458 | -0.153 ± 0.004 |
| $e_p \leq 0.20$ | 28019 | -0.144 ± 0.002 |

3.4 Comparing Radial Metallicity Gradients using R_{gc} and R_m

Tables 3 and 4 show that the radial metallicity gradient of the RC stars is steeper when considering the current position of the stars (R_{gc}) than that when considering their mean orbit (R_m) in the closest z_{max} to the Galactic plane. One possible interpretation of this is due to a selection effect at the boundaries of our observed regions. At the inner Galactic boundaries of our R_{gc} sample, stars with $R_{gc}-R_m > 0$ can be included in our sample (see Fig. 15). These are higher e_p stars from the inner region that are more metal rich than our R_{gc} -

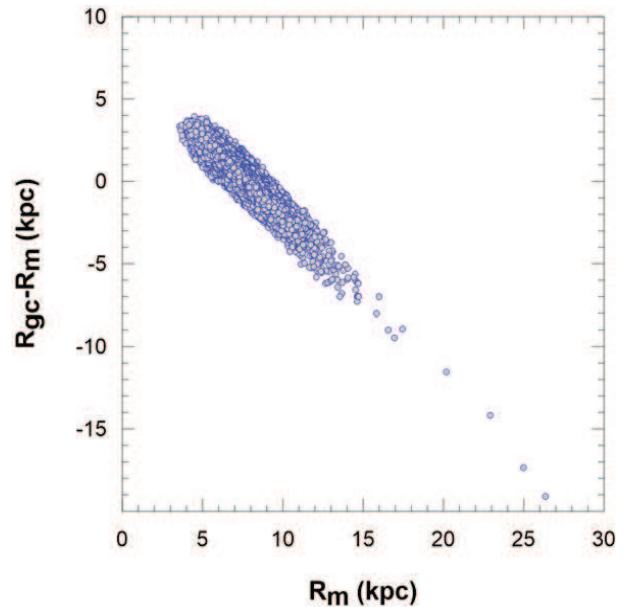


Figure 15. R_m and $R_{gc}-R_m$ diagram.

defined sample. Inclusion of these stars in our sample increases the $[\text{Fe}/\text{H}]$ at the inner Galactic boundaries of our R_{gc} sample.

Similarly, at the outer Galactic boundaries of our R_{gc} sample, stars with $R_{gc}-R_m < 0$ can be included in our sample (see Fig. 15). These are also higher e_p stars from the outer region that are more metal poor than our R_{gc} -defined sample. Inclusion of these stars in our sample decreases the $[\text{Fe}/\text{H}]$ at the outer Galactic boundaries of our R_{gc} sample. These boundary effects steepen the $[\text{Fe}/\text{H}]$ gradient of our R_{gc} -defined sample.

Our R_m -defined sample extends over a wider range of Galactic radii (cf. Figs. 8 and 9) and by averaging over r_a and r_p by definition, this sample avoids these boundary effects and so has a shallower gradient. This effect is not seen in the next $0.5 < z_{max} \leq 1$ kpc interval because the higher fraction of older thin disc stars and thick disc stars in this height interval flattens the gradient, reducing the boundary effect.

4 Discussion and Conclusions

We have investigated the Milky Way Galaxy's radial and vertical metallicity gradients using a sample of 47,406 red clump (RC) stars from the RAial Velocity Experiment (RAVE) Data Release (DR) 4. The largest samples in the literature for investigating radial and vertical metallicity gradients are in Hayden et al. (2014) and Boeche et al. (2014), who analyzed $\sim 20,000$ stars, less than half of our sample.

Our sample was selected using the following constraints: (i) T_{eff} and $\log g$ from the RAVE DR4 were used to select the RC stars, $1 - \sigma$ from the peak density

of the RC; (ii) the proper motions used in their space velocity estimations are available in the UCAC4 catalogue (Zacharias et al., 2013), (ii) the iron abundance is available in the RAVE DR4 catalogue (Kordopatis et al., 2013); (iii) $S/N \geq 40$; and (iv) total space velocity errors would be less or equal to 21 km s^{-1} .

The mean absolute magnitude of the RC stars by Groenewegen (2008) ($M_{K_s} = -1.54 \pm 0.04 \text{ mag}$) is used to determine distances to our sample stars. The resulting distances agree with the RAVE DR4 distances (Binney et al., 2014) of the same stars (mean and standard deviation of difference is 87 and 220 pc respectively). Our photometric method also provides distances to 6185 star (13% of our sample) for which distances are not assigned in RAVE DR4.

The metallicity gradients are calculated with their current orbital positions (R_{gc} and Z) and with their orbital properties (mean Galactocentric distance, R_m and z_{max}), as a function of the distance to the Galactic plane: $d[\text{Fe}/\text{H}]/dR_{gc} = -0.047 \pm 0.003 \text{ dex kpc}^{-1}$ for $0 \leq |Z| \leq 0.5 \text{ kpc}$ and $d[\text{Fe}/\text{H}]/dR_m = -0.025 \pm 0.002 \text{ dex kpc}^{-1}$ for $0 \leq z_{max} \leq 0.5 \text{ kpc}$. This reaffirms the radial metallicity gradient in the thin disc but highlights that gradients are sensitive to the selection effects caused by the difference between R_{gc} and R_m . The radial gradient is flat in the interval 0.5-1 kpc from the plane and then becomes positive for the distances greater than 1 kpc from the plane. Both the radial and vertical metallicity gradients are found to become shallower as the eccentricity of the sample increases.

The radial metallicity gradients in terms of Galactocentric distance, for the interval of $0 \leq |Z| \leq 0.5 \text{ kpc}$, $d[\text{Fe}/\text{H}]/dR_g = -0.047 \pm 0.003 \text{ dex kpc}^{-1}$ is compatible with the one of Boeche et al. (2014), i.e. $d[\text{Fe}/\text{H}]/dR_{gc} = -0.054 \pm 0.004 \text{ dex kpc}^{-1}$ within the errors, estimated for the RC stars with $5.5 < R_{gc} < 11 \text{ kpc}$. The radial metallicity gradient in terms of mean orbital distance, $d[\text{Fe}/\text{H}]/dR_m = -0.025 \pm 0.002 \text{ dex kpc}^{-1}$ is flat relative to the one of Bilir et al. (2012), $d[\text{Fe}/\text{H}]/dR_m = -0.041 \pm 0.007 \text{ dex kpc}^{-1}$ estimated for the RC stars. However, Bilir et al. (2012) restricted the vertical eccentricities of their star sample with $e_v \leq 0.07$. e_v is proportional to z_{max} and steeper gradients are found near the plane.

The vertical metallicity gradient estimated for the present position of all RC stars, $d[\text{Fe}/\text{H}]/d|Z| = -0.219 \pm 0.003 \text{ dex kpc}^{-1}$, is steeper than Boeche et al. (2014)'s, $d[\text{Fe}/\text{H}]/d|Z| = -0.112 \pm 0.007 \text{ dex kpc}^{-1}$. As the vertical metallicity gradient gets steeper further from the plane, our steeper result suggests we are sampling a higher number of stars further from the plane than Boeche et al. (2014).

The vertical metallicity gradient in terms of the z_{max} distance estimated in this study, $d[\text{Fe}/\text{H}]/dz_{max} = -0.157 \pm 0.002 \text{ dex kpc}^{-1}$, is comparable with the one in

Plevne et al. (2015), i.e. $d[\text{Fe}/\text{H}]/dz_{max} = -0.176 \pm 0.039 \text{ dex kpc}^{-1}$. The difference between them may originate in the different z_{max} intervals that the two gradients were evaluated, $0 < z_{max} < 3$ and $0 < z_{max} \leq 0.8 \text{ kpc}$ in our study and in Plevne et al. (2015), respectively. The $d[\text{Fe}/\text{H}]/dz_{max}$ metallicity gradients estimated for the RC stars in Bilir et al. (2012) which are also given in Table 2 are different than the corresponding one in our study, due to additional constraints in Bilir et al. (2012).

Table 5 shows that the radial metallicity gradient depends on the eccentricity. Actually, the flat value of $d[\text{Fe}/\text{H}]/dR_m = -0.025 \pm 0.002 \text{ dex kpc}^{-1}$ could be reduced to steeper values, -0.089 ± 0.010 , -0.072 ± 0.007 , -0.053 ± 0.004 and $-0.044 \pm 0.002 \text{ dex kpc}^{-1}$ by applying constraints $e_p \leq 0.05$, 0.07 , 0.10 and 0.20 in $0 \leq z_{max} \leq 0.5 \text{ kpc}$ distance interval, respectively. By this limitation, low e_p steepen the gradients compared to including higher e_p . This could be due to many effects. e_p is expected to increase with age and older stars tend to be more metal-poor so including higher e_p stars includes more metal-poor stars, which will flatten the gradient. Similarly, thick disc stars tend to have higher e_p than thin disc stars so including higher e_p stars includes more thick disc stars, which also tend to be more metal-poor, again flattening the gradient.

We plotted the RC stars in the sub-samples defined by their e_p eccentricities in four Toomre diagrams and investigated their behaviour in terms of space velocities. The Toomre diagrams in Fig. 16 cover the RC stars with distances $0 \leq z_{max} \leq 0.5$, $0.5 < z_{max} \leq 1$, $1 < z_{max} \leq 2$, and $z_{max} > 2 \text{ kpc}$. There is a trend between the space velocity components U and W , and the e_p eccentricities of the stars in all panels, i.e. $(U^2 + W^2)^{1/2}$ increases with increasing e_p . Surprisingly, the total space velocity remains constant, which it suggests that the rotational velocity of the RC sample decreases with increasing z_{max} distances. On the contrary, $(U^2 + W^2)^{1/2}$ velocities of the stars for a given sub-sample increase with increasing z_{max} distances. For example, $(U^2 + W^2)^{1/2} \leq 50 \text{ km s}^{-1}$ for the stars with $e_p \geq 0.20$ in the $0 \leq z_{max} \leq 0.5$ interval, while it is $(U^2 + W^2)^{1/2} < 100 \text{ km s}^{-1}$ in the $1 < z_{max} \leq 2$ interval. Thus, we can say that the space velocity components of the RC stars at the same z_{max} distance, but with different e_p eccentricities, are different. The same argument holds for the stars with the same eccentricities with different z_{max} distances. If we assume that different velocities originate from the intergalactic gas clouds of different angular momentum as well as different chemical structure, then we can expect different metallicity gradients for different sub-samples, as in case of this study.

These findings can be used to constrain different formation scenarios of the thick and thin discs. The next

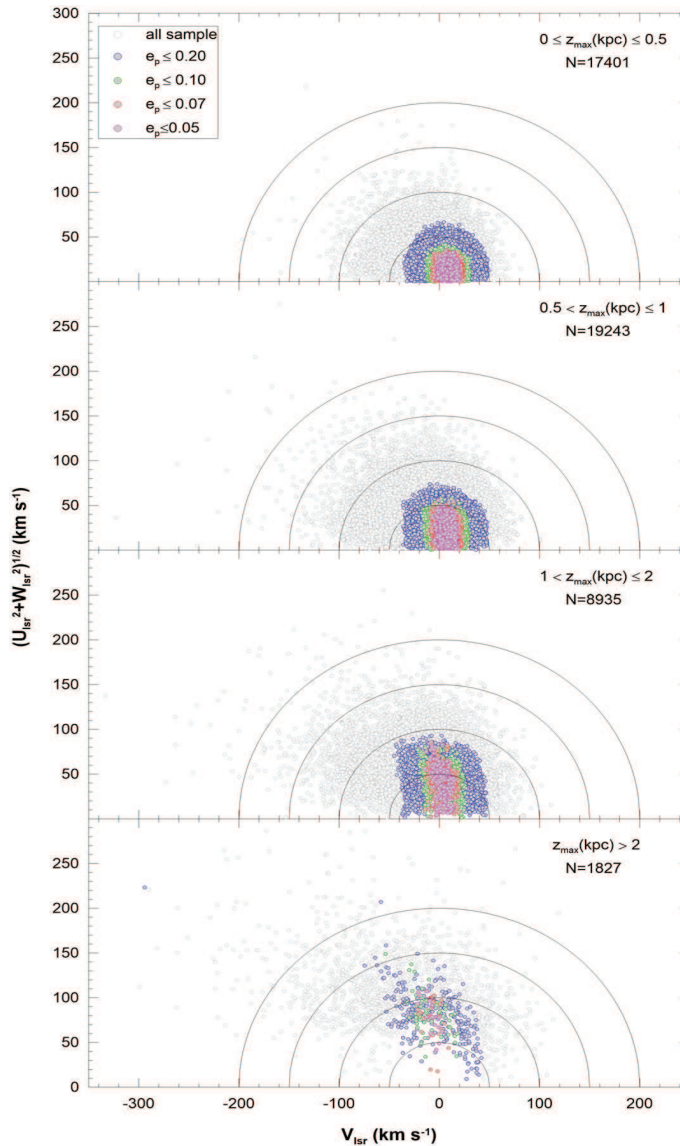


Figure 16. Toomre energy diagram of 47,406 RC stars in four z_{max} intervals. Pink, red, green, blue and grey circles represent $e_p \leq 0.05$, $e_p \leq 0.07$, $e_p \leq 0.10$, $e_p \leq 0.20$ and $e_p \leq 1$ samples. Black solid lines show total space velocity borders of 50, 100 and 150 km s^{-1} , respectively.

step will be to repeat this analysis with improved astrometry, including trigonometric parallaxes, measured by *Gaia*. *Gaia*'s first data release will include these measurements for Tycho-2 stars (Michalik et al., 2015), which are the brighter half of RAVE stars.

5 Acknowledgments

Authors are grateful to the anonymous referee for his/her considerable contributions to improve the paper. This study has been supported in part by the Scientific and Technological Research Council (TÜBİTAK) 114F347 and the Research Fund of the University of

Istanbul, Project Number: 36224. This research has made use of NASA's (National Aeronautics and Space Administration) Astrophysics Data System and the SIMBAD Astronomical Database, operated at CDS, Strasbourg, France and NASA/IPAC Infrared Science Archive, which is operated by the Jet Propulsion Laboratory, California Institute of Technology, under contract with the National Aeronautics and Space Administration.

REFERENCES

- Allende, P. C., Carlos, B., Timothy, C., et al., 2006, *ApJ*, 636, 804
- Alves, D. R., 2000, *ApJ*, 539, 732
- Ak, S., Bilir, S., Karaali, S., Buser, R., 2007a, *AN*, 328, 169
- Ak, S., Bilir, S., Karaali, S., Buser, R., Cabrera-Lavers, A., 2007b, *NewA*, 12, 605
- Andreuzzi, G., Bragaglia, A., Tosi, M., Marconi, G., 2011, *MNRAS*, 412, 1265
- Andrievsky, S. M., Kovtyukh, V. V., et al., 2002, *A&A*, 392, 491
- Bahcall, J. N., Soneira, R. M., 1980, *ApJS*, 44, 73
- Bartašiūtė, S., Aslan, Z., Boyle, R. P., 2003, *BaltA*, 12, 539
- Bergemann, M., Ruchti, G. R., Serenelli, A., et al., 2014, *A&A*, 565, A89
- Bijaoui, A., Recio-Blanco, A., de Laverny, P., Ordenovic, C., 2012, *Statistical Methodology*, 9, 55
- Bilir, S., Karaali, S., et al., 2008, *MNRAS*, 390, 1569
- Bilir, S., Karaali, S., Ak, S., Önal, Ö., Dağtekin, N. D., et al., 2012, *MNRAS*, 421, 3362
- Bilir, S., Önal, Ö., Karaali, S., Cabrera-Lavers, A., Çakmak, H., 2013a, *Ap&SS*, 344, 417
- Bilir, S., Ak, T., Ak, S., Yontan, T., Bostanci, Z. F., 2013b, *NewA*, 23, 88
- Binney, J., Burnett, B., et al., 2014, *MNRAS*, 437, 351
- Boeche, C., Siebert, A., et al., 2013, *A&A*, 559A, 59
- Boeche, C., Siebert, A., et al., 2014, *A&A*, 568A, 71
- Bovy, J., 2015, *ApJS*, 216, 29
- Burnett, B., Binney, J., 2010, *MNRAS*, 407, 16
- Cabrera-Lavers, A., Garzón, F., Hammersley, P. L., 2005, *A&A*, 433, 173
- Cabrera-Lavers, A., Hammersley, P.L., González-Fernández, C., López-Corredoira, M., Garzón, F., Mahoney, T. J., 2007a, *A&A*, 465, 825
- Cabrera-Lavers, A., Bilir, S., Ak, S., Yaz, E., López-Corredoira, M., 2007b, *A&A*, 464, 565
- Cabrera-Lavers, A., González-Fernández, C., Garzón, F., Hammersley, P. L., López-Corredoira, M., 2008, *A&A*, 491, 781
- Cannon, R. D., 1970, *MNRAS*, 150, 111
- Carrell, K., Chen, Y., Zhao, G., 2012, *AJ*, 144, 185
- Carretta, E., Gratton, R., Sneden, C., Bragaglia, A., 1999, *Ap&SS*, 265, 189

- Chen, L., Hou, J. L., Wang, J. J., 2003, *AJ*, 125, 1397
- Chen, Y. Q., Zhao, G., Carrell, K., Zhao, K., 2011, *AJ*, 142, 184
- Cheng, J. Y., et al., 2012, *ApJ*, 746, 149
- Coşkunoğlu, B., et al., 2011, *MNRAS*, 412, 1237
- Coşkunoğlu, B., Ak, S., et al., 2012, *MNRAS*, 419, 2844
- Cunha, K., Frinchaboy, P. M., et al., 2016, *AN*, in press, arXiv:1601.03099
- Cutri, R. M., et al., 2003, 2MASS All-Sky Catalog of Point Sources, CDS/ADC Electronic Catalogues, 2246
- Eggleton, B. B., 1968, *MNRAS*, 140, 387
- ESA, 1997, The Hipparcos and Tycho Catalogues, ESA SP-1200. ESA, Noordwijk
- Friel, E. D., Janes, K. A., et al., 2002, *AJ*, 124, 2693
- Friel, E. D., Jacobson, H. R., Pilachowski, C. A., 2010, *AJ*, 139, 1942
- Frinchaboy, P. M., Thompson, B., et al., 2013, *ApJ*, 777, 1
- Genovali, K., Lemasle, B., et al., 2014, *A&A*, 566, 37
- Gilmore, G., Randich, S., et al., 2012, *Msngr*, 147, 25
- Girard, T. M., van Altena, W. F., et al., 2011, *AJ*, 142, 15
- Girardi, L., 1999, *MNRAS*, 308, 818
- Groenewegen, M. A. T., 2008, *A&A*, 488, 25
- Hayden, M. R., et al., 2014, *AJ*, 147, 116
- Haywood, M., 2008, *MNRAS*, 388, 1175
- Hog, E., et al., 2000, *A&A*, 355L, 27
- Hou, J., Chang, R., Chen, L., 2002, *ChJAA*, 2, 17
- Huang, Y., Liu, X.-W., et al., 2015, *RAA*, 15, 1240
- Iben, I., Jr., 1991, *ApJS*, 76, 55
- Jacobson, H. R., D. Friel, E. D., et al., 2016, *A&A*, 591, 37
- Johnson, D. R. H., Soderblom, D. R., 1987, *AJ*, 93, 864
- Jurić, M., Ivezić, Z., Brooks, A., et al., 2008, *ApJ*, 673, 864
- Karaali, S., Ak, S. G., Bilir, S., Karataş, Y., Gilmore, G., 2003, *MNRAS*, 343, 1013
- Karaali, S., Bilir, S., Yaz Gökçe, 2013, *Ap&SS*, 344, 417
- Karataş, Y., Klement, R. J., 2012, *NewA*, 17, 22
- Katz, D., Soubiran, C., Cayrel, R., Barbuy, B., Friel, E., Bienayme, O., Perrin, M.-N., 2011, *A&A*, 525A, 90
- Keenan, P. C., Barnbaum, C., 1999, *ApJ*, 518, 859
- Kordopatis, G., Recio-Blanco, A., et al., 2011, *A&A*, 535, 107
- Kordopatis, G., Gilmore, G., et al., 2013, *AJ*, 146, 134
- Laney, C. D., Joner, M. D., Pietrzyński, G., 2012, *MNRAS*, 419, 1637
- Lemasle, B., François, P., et al., 2007, *A&A*, 467, 283
- Lemasle, B., François, P., et al., 2008, *A&A*, 490, 613
- López-Corredoira, M., Cabrera-Lavers, A., Garzón, F., Hammersley, P. L., 2002, *A&A*, 394, 883
- López-Corredoira, M., Cabrera-Lavers, A., Gerhard, O., Garzón, F., 2004, *A&A*, 421, 953
- Luck, R. E., Andrievsky, S. M., Kovtyukh, V. V., Gieren, W., Graczyk, D., 2011, *AJ*, 142, 51
- Luck, R. E., Lambert, D. L., 2011, *AJ*, 142, 136
- Magrini, L., Sestito, P., Randich, S., Galli, D., 2009, *A&A*, 494, 95
- Majewski, S. R., Wilson, J. C., Hearty, F., Schiavon, R. R., Skrutskie, M. F., 2010, *AJ*, 151, 12
- Marsakov, V. A., Borkova, T. V., 2006, *A&AT*, 25, 157
- Michalik, D., Lindegren, L., Hobbs, D., 2015, *A&A*, 574, A115
- Mikolaitis, Š., Hill, V., Recio-Blanco, A., et al., 2014, *A&A*, 572, A33
- Mihalas, D., Binney, J., 1981. in *Galactic Astronomy*, 2nd edition, Freeman, San Fransisco
- Netopil, M., Paunzen, E., Heiter, U., Soubiran, C., 2016, *A&A*, 585A, 150
- Nordström, B., Mayor, M., et al., 2004, *A&A*, 418, 989
- Paczynski, B., Stanek, K. Z., 1998, *ApJ*, 494L, 219
- Pedicelli, S., Bono, G., et al., 2009, *A&A*, 504, 81
- Peng, X., Du, C., Wu, Z., 2012, *MNRAS*, 422, 2756
- Plevne, O., Ak, T., et al., 2015, *PASA*, 32, 43
- Recio-Blanco, A., Bijaoui, A., de Laverny, P., 2006, *MNRAS*, 370, 141
- Recio-Blanco, A., de Laverny, P., Kordopatis, G., et al., 2014, *A&A*, 567, A5
- Roeser, S., Demleitner, M., Schilbach, E., 2010, *AJ*, 139, 2440
- Ruchti, G. R., Fulbright, J. P., et al., 2011, *ApJ*, 737, 9.
- Schlafly, E. F., Finkbeiner, D. P., 2011, *ApJ*, 737, 103
- Schlesinger, K. J., Johnson, J. A., et al., 2014, *ApJ*, 791, 112
- Schönrich R., 2012, *MNRAS*, 427, 274
- Siebert, A., Williams, M. E. K., et al., 2011, *AJ*, 141, 187
- Siegel, M. H.; Karataş, Y., Reid, I. N., 2009, *MNRAS*, 395, 1569
- Skrutskie, M. F., et al., 2006, *AJ*, 131, 1163
- Soubiran, C., Bienayme, O., Mishenina, T. V., Kovtyukh, V. V., 2008, *A&A*, 480, 91
- Steinmetz, M., Zwitter, T., et al., 2006, *AJ*, 132, 1645
- Thomas, H. C., 1967, *Zs. Ap.*, 67, 420
- Udalski, A., 2000, *ApJ*, 531L, 25
- Williams, M. E. K., Steinmetz, M., Binney, J., et al., 2013, *MNRAS*, 436, 101
- Wilson, M. L., Helmi, A., Morrison, H. L., et al., 2011, *MNRAS*, 413, 2235
- Wu, Z., Zhou, X., Ma, J., Du, C., 2011, *MNRAS*, 413, 2235
- Xiang, M., Liu, X. W., Yuan, H. B., et al., 2015, *RAA*, 15, 1209
- Yanny, B., Rockosi, C., et al., 2009, *AJ*, 137, 4377
- Yaz, E., Karaali, S., 2010, *NewA*, 15, 234
- Yaz Gökçe, E., Bilir, S., et al., 2013, *NewA*, 25, 19
- Yong, D., Carney, B. W., Friel, E. D., 2012, *AJ*, 144, 95
- Zacharias, N., Finch, C., et al., 2010, *AJ*, 139, 2184

- Zacharias, N., Finch, C. T., et al., 2013, *AJ*, 145, 44
Zhao, G., Zhao, Y., Chu, Y., Jing, Y., Deng, L., 2012,
 RAA, 12, 723
Zucker, D. B., de Silva, G., et al., 2012, *ASPC*, 458, 421
Zwitter, T., Matijević, et al., 2010, *A&A*, 522, 54